THE JOURNAL OF COMPARATIVE NEUROLOGY 325:169–182 (1992)

Three-Dimensional Analysis of the Structure and Composition of CA3 Branched Dendritic Spines and Their Synaptic Relationships With Mossy Fiber Boutons in the Rat Hippocampus

MARINA E. CHICUREL AND KRISTEN M. HARRIS
Department of Neurology Research, Children's Hospital, and Program in Neuroscience, Harvard Medical School, Boston, Massachusetts 02115

ABSTRACT

This paper is the third in a series to quantify differences in the composition of subcellular organelles and three-dimensional structure of dendritic spines that could contribute to their specific biological properties. Proximal apical dendritic spines of the CA3 pyramidal cells receiving synaptic input from mossy fiber (MF) boutons in the adult rat hippocampus were evaluated in three sets of serial electron micrographs. These CA3 spines are unusual in that they have from 1 to 16 branches emerging from a single dendritic origin. The branched spines usually contain subcellular organelles that are rarely found in adult spines of other brain regions including ribosomes, multivesicular bodies (MVB), mitochondria, and microtubules. MVBs occur most often in the spine heads that also contain smooth endoplasmic reticulum, and ribosomes occur most often in spines that have spinules, which are small nonsynaptic protuberances emerging from the spine head.

Most of the branched spines are surrounded by a single MF bouton, which establishes synapses with multiple spine heads. The postsynaptic densities (PSDs) occupy about 10–15% of the spine head membrane, a value that is consistent with spines from other brain regions, with spines of different geometries, and with immature spines. Individual MF boutons usually synapse with several different branched spines, all of which originate from the same parent dendrite. Larger branched spines and MF boutons are more likely to synapse with multiple MF boutons and spines, respectively, than smaller spines and boutons.

Complete three-dimensional reconstructions of representative spines with 1, 6, or 12 heads were measured to obtain the volumes, total surface areas, and PSD surface areas. Overall, these dimensions were larger for the complete branched spines than for unbranched or branched spines in other brain regions. However, individual branches were of comparable size to the large mushroom spines in hippocampal area CA1 and in the visual cortex, though the CA3 branches were more irregular in shape. The diameters of each spine branch were measured along the cytoplasmic path from the PSD to the origin with the dendrite, and the lengths of branch segments over which the diameters remained approximately uniform were computed for subsequent use in biophysical models. No constrictions in the segments of the branched spines were thin enough to reduce charge transfer along their lengths. The complex geometry of these spines and their subcellular constituents could modulate postsynaptic responses, however, during synaptic activation or plasticity such as long term potentiation, in ways that can now be evaluated on the basis of the complete dimensions and descriptions reported here.

Key words: serial electron microscopy, ribosomes, microtubules, multivesicular bodies, postsynaptic density, modeling, reconstruction

Dendritic spines are the clearest example of a postsynaptic element whose structure can have a direct effect on synaptic transmission and integration. Unfortunately, dendritic spines are small and inaccessible, and therefore,

Accepted June 10, 1992.

Address reprint requests to Kristen M. Harris, Ph.D., Department of Neurology Research, Children's Hospital, Enders 208, 300 Longwood Ave., Boston, MA 02115.

direct physiological recordings have not been obtained. Theoretical models have been created to predict how dendritic spine structure could influence synaptic transmission and molecular compartmentation (e.g., Rall '70, '74, '78; Diamond et al., '70; Koch and Poggio, '83; Kawato et al., '84; Wilson, '84; Turner, '84; Coss and Perkel, '85; Gamble and Koch, '87; Brown et al., '88; Wickens, '88; Rall and Segev, '88). All of these models require exact anatomical dimensions for accurate interpretation of their predictions. The dendritic spines of hippocampal CA3 pyramidal cells that form synapses with the mossy fiber (MF) boutons of the dentate granule cells are an extreme example of the structural complexity that dendritic spines can assume, and therefore have been the most difficult to analyze anatomically.

Ramon y Cajal first discovered contacts between the MF boutons and the proximal dendritic spines of CA3 pyramidal cells in Golgi preparations (Ramon y Cajal, '11). Partial reconstructions from serial electron microscopy (EM) revealed these dendritic spines to be unique in the central nervous system (CNS) in their complex subcellular composition and highly branched morphology (Blackstad and Kjaerheim, '61). Additional analyses have confirmed these observations and have further elucidated the complex morphology and composition of the presynaptic MF bouton (Hamlyn, '61, '62, Bliss et al., '74; Amaral, '79; Amaral and Dent, '81; Frotscher, '85; Gaarskjaer, '86). These MF boutons contain glutamate (Storm-Mathisen et al., '83; Terrian et al., '88, '90), at least four different dynorphin-derived peptides (McGinty et al., '83; Hoffman and Zamir, '84; Terrian et al., '88, '90), ATP (Terrian et al., '89), high concentrations of zinc (Ibata and Otsuka, '69), and GABA (Sandler and Smith, '91). There is evidence for differential release of these neurotransmitters that may be modulated by adenosine and arachidonic acid (Terrian et al., '89; Freeman et al., '90). Release may also be modulated by changes in gene expression, as seems to be the case for the enkephalin and dynorphin peptides (Morris et al., '88; Gall, '88). To determine whether the releasable substances of a single MF are likely to have access to one or more CA3 cells, single MF boutons were examined through serial sections to ascertain whether they synapse with one or more branched spines and whether the different spines come from the same or different neurons.

The distance from the MF synapses to the CA3 cell soma is sufficiently short to be considered electrotonically negligible (Johnston and Brown, '83); therefore, quantal analyses and estimates of single synaptic conductances can be more readily obtained from recordings in the CA3 cell soma than for other CNS spine synapses that are usually located more distally (Barrionuevo et al., '86; Xiang et al., '90). Long-term potentiation (LTP), an enduring form of synaptic potentiation, is induced by appropriate stimulation of the MF-CA3 synapse, where the mechanisms of *induction* (Harris and Cotman, '86; Hopkins and Johnston, '88; Williams and Johnston, '88; Ito et al., '88; Kamiya et al., '88; Okada et al., '89; Williams and Johnston, '89; Jaffe and Johnston, '90; Zalutsky and Nicoll, '90) and *expression* (Bradler and Barrionuevo, '89, '90; Staubli et al., '90; Regehr and Tank, '91) differ from other hippocampal synapses. For example, induction of LTP at the MF-CA3 synapse is not blocked by NMDA receptor antagonists (Harris and Cotman, '86). The available physiological data also suggest that the maintenance of LTP has both pre- and postsynaptic components (Williams and Johnston, '89; Zalutsky and Nicoll, '90; Jaffe and Johnston, '90). The role(s) that changes in the postsynaptic branched spines could play in modulating LTP at the MF-CA3 synapse remains unknown. Early results from single section analyses have suggested that these spines, their smooth endoplasmic reticulum (SER), and the SER in the MF bouton swell, though no information is available on their branching patterns or overall dimensions following establishment of LTP (Moshkov et al., '77; Petukhov and Popov, '86). In addition, MF sprouting has been revealed through light microscopy of the Timm's stain, to be associated with seizure episodes in both young and adult animals (for review see Ben-Ari and Represa, '90).

Complete measurements of the dimensions of the MF-CA3 synaptic complex are required to understand the physiological consequences of their highly branched structure. With these data, the predictions of theoretical models can be tested and revised to account for the physiological findings (Wilson, '84; Harris and Stevens, '88, '89; Amaral et al., '90). In the past, the dimensions of the MF-CA3 synapse have been estimated from single thin sections or from partial reconstructions. In the present study the complete dimensions of a representative sample of MF-CA3 branched spines and their synapses were obtained through complete reconstructions from serial EM. The measurements of their dimensions, along with descriptions of their subcellular composition, are provided in sufficient detail to allow for accurate modeling of their biophysical properties.

MATERIALS AND METHODS

Tissue preparation

Hippocampal area CA3 was obtained from a young adult male rat of the Long-Evans strain (310 g, approx. 70 days old); dendrites of cerebellar Purkinje cells and hippocampal CA1 pyramidal cells have also been analyzed in previous studies using this rat (Harris and Stevens, '88, '89). Perfusion and tissue processing were done as previously described (Harris and Stevens, '89). Briefly, perfusion through the heart was performed under deep pentobarbital anesthesia with 2% paraformaldehyde and 2.5% glutaraldehyde in 0.1 M cacodylate buffer with 2 mM $CaCl_2$. The hippocampus was removed and sectioned into 400 μm thick slices. These slices were rinsed in buffer and then soaked in 1% OsO_4 with 1.5% $K_4Fe(CN)_6$ for 1 hour followed by immersion in OsO_4 for an additional hour. The slices were then rinsed in buffer, soaked for 5 minutes each in 30% and 50% ethanol, immersed for 1 hour in 1% uranyl acetate in 70% ethanol, dehydrated through graded ethanols and propylene oxide, and embedded in Epon. Blocks were trimmed to contain the hippocampal CA3 pyramidal cell bodies and their apical dendrites in stratum lucidum. Serial sections were cut on a Reichert Ultracut E ultramicrotome, mounted on Formvar-coated slot grids (Synaptek) and stained for 5 minutes with Reynolds' lead citrate.

Electron microscopy

Each grid was put into a grid cassette (Stevens and Trogadis, '84), mounted on a modified rotating stage (JEOL SRH-10Mod) to obtain consistent orientation of adjacent

sections, and photographed at a JEOL 1200EX electron microscope. Three samples located approximately 30 μm from the CA3 pyramidal cell layer in stratum lucidum were photographed at 6,000 magnification through serial sections. Two samples had 60 serial sections each and the other had 27 sections (total = 147 sections). All of the branched spines having a postsynaptic density (PSD) intersected by the middle section of a series were viewed through serial sections to quantify the number of heads, to determine which heads had PSDs, to identify their subcellular constituents, and to determine the number and size of the MF boutons synapsing with them.

Three-dimensional (3-D) reconstructions

The methods described in Stevens and Trogadis ('84), Harris and Stevens ('88) and Harris et al. ('92) were used to obtain complete 3-D reconstructions of CA3 branched spines. Section thickness was estimated by measuring the diameters of longitudinally sectioned mitochondria and then counting the number of sections the mitochondria appeared in; thus (μm/section) = measured diameter (μm)/number of sections. An average section thickness of 0.08 μm was obtained for these series.

To align branched spine contours in adjacent sections, the image of the electron micrograph from one section viewed through a video camera was stored in the Gould frame buffer interfaced to a VAX 11/780 computer. The image of the adjacent section was viewed "live" with the camera and moved while flickering the stored image until the branched spine contours and all of the surrounding structures were superimposed. The new images were then traced.

Graphics editing

In general, the procedures described in Harris and Stevens ('88) were used to reconstruct, edit, and quantify the dimensions of the branched spines with the PANDORA image-analysis system (Pearlstein et al., '86). Each reconstructed branched spine was first rotated about its central axis to discern where to cut the junction between the origin of the branched spine and its parent dendrite. The average-sized branched spine was further edited into its head, primary branch, and higher-order branch compartments. In this case, rotation of the reconstructed structure was also used to obtain different viewing angles. After removing the parent dendrite, the branched spine was edited into its secondary branches. Each secondary branch with its corresponding heads and branches was then displayed and rotated separately to create separate compartments and to measure their volumes and surface areas.

Computation of areas, volumes and lengths

The *surface areas* of the reconstructed branched spines were calculated by interpolating the contour perimeters between adjacent sections, multiplying by the section thickness and adding the areas of plasmalemma cut en face. If two adjacent sections contained plasmalemma areas cut en face, a connector was drawn where the areas overlapped across sections. The areas associated with the connectors were interpolated between adjacent sections. Then the following formula was used for calculating total surface areas, compartment surface areas and PSD areas:

$$\textit{Surface area} = \Sigma_{i=1}^{n} |(p_i + (p_{i+1} - p_i)/2) \times \text{section thickness}| + \text{en face membrane areas, where:}$$

p_i and p_{i-1} represent perimeter values of adjacent sections, and

n = number of sections that the subject traversed.

The *volumes* were computed by multiplying the area of traced cytoplasm by the section thickness. Volumes at spine boundaries, where part of the plasmalemma was cut en face, were computed by multiplying the area of membrane by section thickness and dividing by 2 because it was assumed that cytoplasm occurred under about half of the membrane area in the last section.

To calculate *lengths* from PSDs to spine origins, a line was traced from the center of each PSD through the center of each branch traversed to reach the spine origin. This was accomplished by viewing of individual, superimposed serial images from adjacent sections and by rotating the full reconstruction of the branched spine about its central axis to view it from all angles. All the lengths of lines traversing longitudinally sectioned areas of cytoplasm were summed; lengths of lines going through cross- or obliquely sectioned areas of cytoplasm were interpolated by the Pythagorean theorem:

$$\textit{interpolated length} = \sqrt{(t^2 + l^2)}$$

where: t = section thickness and

l = the length of the line along the displacement from 1 section to the next.

The sum of the longitudinal and cross-sectional distances yielded the total length. These lengths were subdivided into segments where the diameters of the spine remained approximately uniform. Representative diameters of the constrictions were calculated in the middle of the segment in the same way as the other lengths.

Sphericality index

As a measurement of the degree of irregularity in the spine head shape the following formula was used: $\textit{sphericality index} = 6(\pi^{1/2}\,\textit{Volume})/(\textit{Surface Area})^{3/2}$. A sphericality index of 1 indicates a perfectly spherical shape; the lower the value, the greater the irregularity in the head surface.

Statistical analyses

The RS1 statistical package (Bolt, Beranek and Newman, Cambridge, MA) was used to obtain χ^2 values and correlations as described in the Results. Associations between organelles in a single spine head were revealed by testing through the χ^2 analysis. Since the comparisons done lacked independence, the Dunn-Sidak method (Sokal and Rohlf, '81) was used to obtain an alpha value equivalent to 0.05 and:

$$alpha' = 1 - (1 - alpha)^{1/k},$$

where: $alpha'$ = the corrected alpha value, and

k = the number of degrees of freedom.

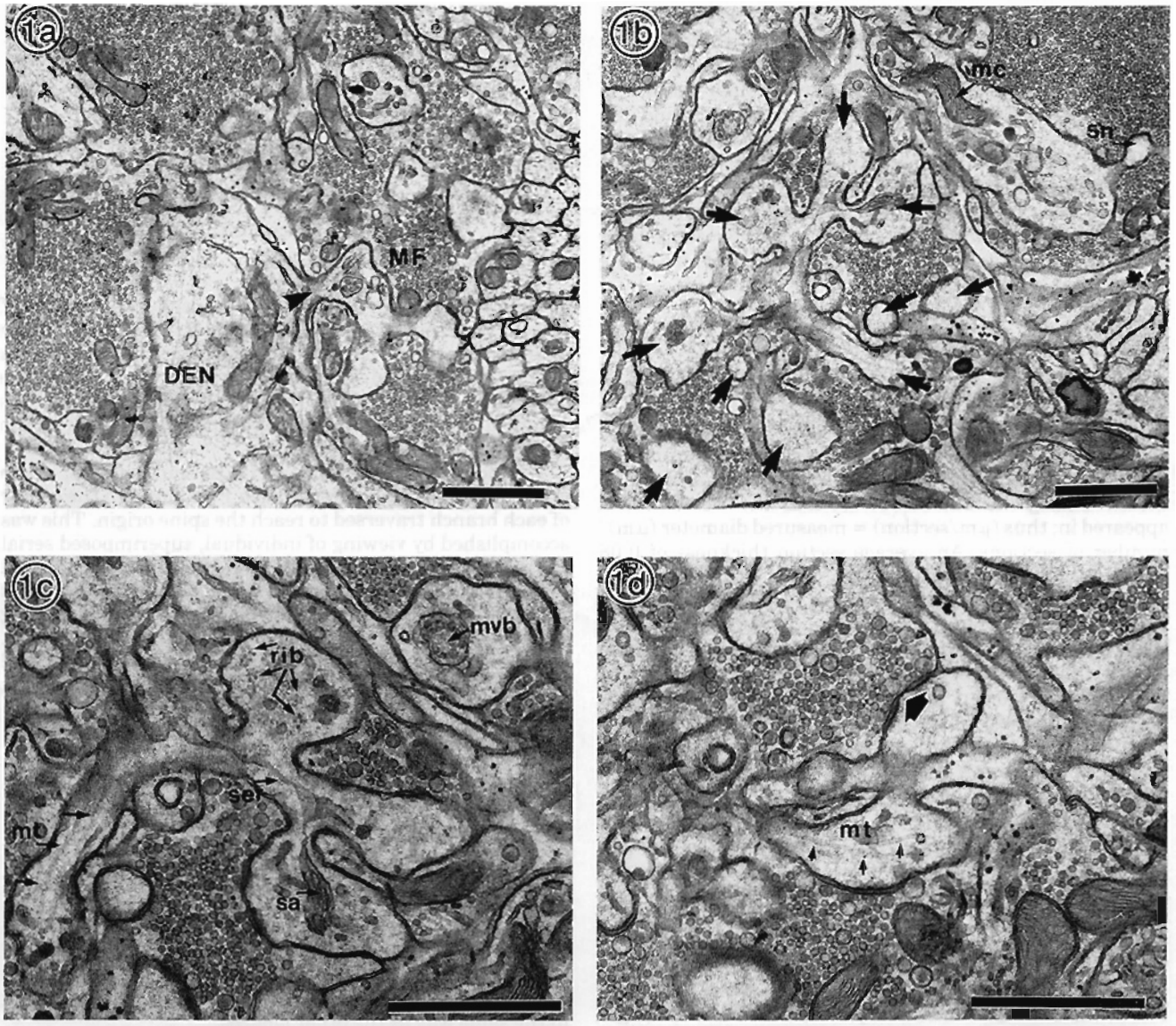

Fig. 1. Ultrastructural characteristics of CA3 branched spines. **a:** CA3 branched spine connected to its parent dendrite (DEN). The origin is at the arrowhead. Mossy fiber bouton cytoplasm is also indicated (MF). **b:** Branching pattern of a CA3 spine. Heads belonging to this branched spine are labelled with arrows. A spinule (sn) and mitochondrion (mc) occur in the head of a different spine. **c** and **d:** Ribosomes (rib), microtubules (mt), smooth endoplasmic reticulum (ser), spine apparatus (sa), and multivesicular bodies (mvb) are shown at higher magnification. The perforation in a post synaptic density (PSD) in d is indicated by a large arrow. Bars = 1 μm.

The correlation between the total number of heads on a branched spine and the fraction of those heads containing each of the organelles was obtained by computing r and testing whether r was significantly different from zero.

RESULTS

Ultrastructure of the CA3 branched dendritic spines and their associated mossy fiber (MF) boutons

The CA3 branched spine emerges from the parent dendrite as a single constricted neck that gives rise to secondary branches and extensions that expand into bulbous and irregularly shaped "heads" (Fig. 1a,b). Most of the heads have a thickened PSD separated from the presynaptic terminal by a widened synaptic cleft containing dense staining material (Fig. 1c,d). When viewed through serial sections, some of these PSDs form a continuous macula on a smooth membrane. Other PSDs have complex morphologies, occurring on undulating membranes, and perforated by electron lucent regions (Fig. 1d). Occasionally, a spinule, characterized by a thin stalk with a tiny swelling, extends from a spine head into the MF bouton (Fig. 1b).

The ultrastructural constituents of the branched spines are distinctly numerous and varied. SER is present throughout most portions of the branched spines. The classical spine apparatus, which has flattened sacs of SER laminated between dense-staining material, is found in some spine branches (Figs. 1c, 2a). Some branched spines contain ribosomes, multivesicular bodies (MVBs), mitochondria,

and microtubules. Ribosomes occur frequently in these spines, and are usually arranged in small clusters of three to six granules (Fig. 1c). MVBs are spherical, membrane-bound structures containing a variable number of smaller vesicles (Figs. 1c, 2a). Mitochondria of various sizes and shapes occur in some of the branched spines (Figs. 1b, 2a), and microtubules extend from the dendrite into portions of some of the branched spines (Fig. 1d).

These CA3 branched spines invaginate the vesicle-rich presynaptic boutons of the MF. On single sections, several portions of an individual branched spine appear with each bouton (Figs. 1b, 2a). The MF boutons contain many small clear vesicles, fewer dense core vesicles and even fewer large clear vesicles. Mitochondria cluster near the plasma membrane of the bouton such that distinct vesicular and mitochondrial domains can be identified (Fig. 2a). Occasionally, synapses are formed between the MF boutons and dendritic shafts. However, usually the apposing junctional thickenings have no vesicles and are referred to as puncta adherentia (Fig. 2b).

Quantitative evaluation of the subcellular constituents in the CA3 branched spines

Twenty complete branched spines were evaluated through serial sections. All 20 had PSDs and SER in at least one branch or head, while 19 had ribosomes, 17 had MVBs, 16 had spinules, 11 had mitochondria and 8 had microtubules (Fig. 3a). The number of heads per branched spine ranged from 1 to 16 with a mean ± S.D. of 7 ± 4 heads. The ultrastructural components were quantified in each of 134 complete heads on the 20 complete branched spines, and 71 complete heads on an additional 9 incomplete (i.e., not entirely contained within the series of photographed sections) branched spines for a total of 205 heads on 29 branched spines. The ultrastructural components occurred in the same order of abundance in the individual heads as in the whole spines (Fig. 3b). Spinules were found to be associated with the presence of ribosomes ($\chi^2 = 15.75$, $df = 21$, $p < 0.005$), and MVBs were found to be associated with the presence of SER ($\chi^2 = 6.40$, $df = 21$, $p < 0.05$) in the same spine head. The small fraction of spine heads that did not have SER in them tended to occur on highly branched spines ($r = 0.55$, $p < 0.005$). In addition, the highly branched spines were more likely to have microtubules in some of their heads than spines with fewer heads ($r = 0.38$; $p < 0.05$).

Associations between MF boutons and CA3 branched spines

The number of MF boutons contacted by the 20 complete and 9 incomplete branched spines was determined. For 17 spines, all of the heads synapsed with a single bouton; for 3 spines different heads synapsed with two boutons; and for 1 incomplete spine the different heads synapsed with at least three boutons. Thus, while most branched spines synapse with only one bouton, a few synapse with more than one bouton. All of the spines synapsing with more than one MF bouton had a greater than average number of heads.

Seventeen MF boutons were found to make synapses with at least 1 head of the sampled branched spines. These MF boutons were grouped by size as large ($n = 4$) or medium to small ($n = 13$) (see Fig. 2a). Their size was assigned on the section with the maximal cross-sectional area. Fourteen spines synapsed with large boutons, and only 1 of these synapsed with more than one MF bouton. Of the spines synapsing with medium or small boutons, 3 synapsed with just 1 bouton, 5 synapsed with more than 1 bouton, and 5 were too incomplete to determine whether they synapsed with 1 or more boutons. Thus, spines synapsing with medium or small boutons are more likely to form synapses with multiple MF boutons than spines that synapse with large MF boutons.

Sixteen of these boutons synapsed with heads emerging from more than one branched spine (see Fig. 2a) and one synapsed with the heads of a single branched spine. Only five of the boutons were complete because the MF boutons can have diameters up to 10 μm (Blackstad and Kjaerheim, '61), and our series spanned not more than 4.8 μm. The complete MF boutons were all of the medium to small category. One synapsed with four branched spines for a total of sixteen heads, three synapsed with two branched spines for a total of nine, fifteen, and seventeen heads, while one bouton synapsed with one branched spine that had sixteen heads. The largest number of contacts occurred between a large MF bouton that was incomplete and which contacted at least seven different branched spines for a total of thirty-seven heads. All of the branched spines synapsing with the same MF bouton originated from a single parent dendrite.

3-D reconstructions of CA3 branched spines

Three classes of branched spines were identified in the group of twenty complete spines: those having larger, similar to, and less than average sizes. Size was assigned according to both the number of heads and the number of sections spanned by the whole spine. One spine from each of these groups was then randomly selected for complete 3-D reconstruction and quantification. The "large" spine had twelve heads, the "average" spine had six heads and the "small" spine had a single head (Fig. 4a–f).

Analysis of the 3-D structure of the reconstructed branched spines

The distance from each PSD to the origin of the spine with the parent dendrite and the corresponding diameters of the branches and heads were measured and are represented schematically for modeling purposes (Fig. 5a,b,c, Tables 1–3). In Figure 5, circles represent the PSDs, lines represent the lengths along segments of the spine branches, and a filled rectangle represents the origin with the parent dendrite. The associated tables provide the PSD areas, total lengths from the PSD to the origin with the dendrites, the lengths over which the diameters remain approximately uniform, and the diameters at the lettered positions.

Volumes, surface areas, PSD areas and the ratio of PSD to head membrane area were obtained from the three reconstructed spines and compared to spines from other brain regions (Table 4). The CA3 branched spines have considerably larger total volumes, surface areas and PSD areas than the other spine types, but the average dimensions of individual branches are comparable to the other spines. In addition, the ratio of PSD to head membrane areas are remarkably uniform across the different spine types. The *sphericality index* is the 3-D equivalent of Amaral and Dent's ('81) circularity index and was used to indicate the degree of irregularity in the spine head shape. The sphericality indices of individual heads on the branched spines are considerably lower than those of other spines, indicating their highly irregular shape.

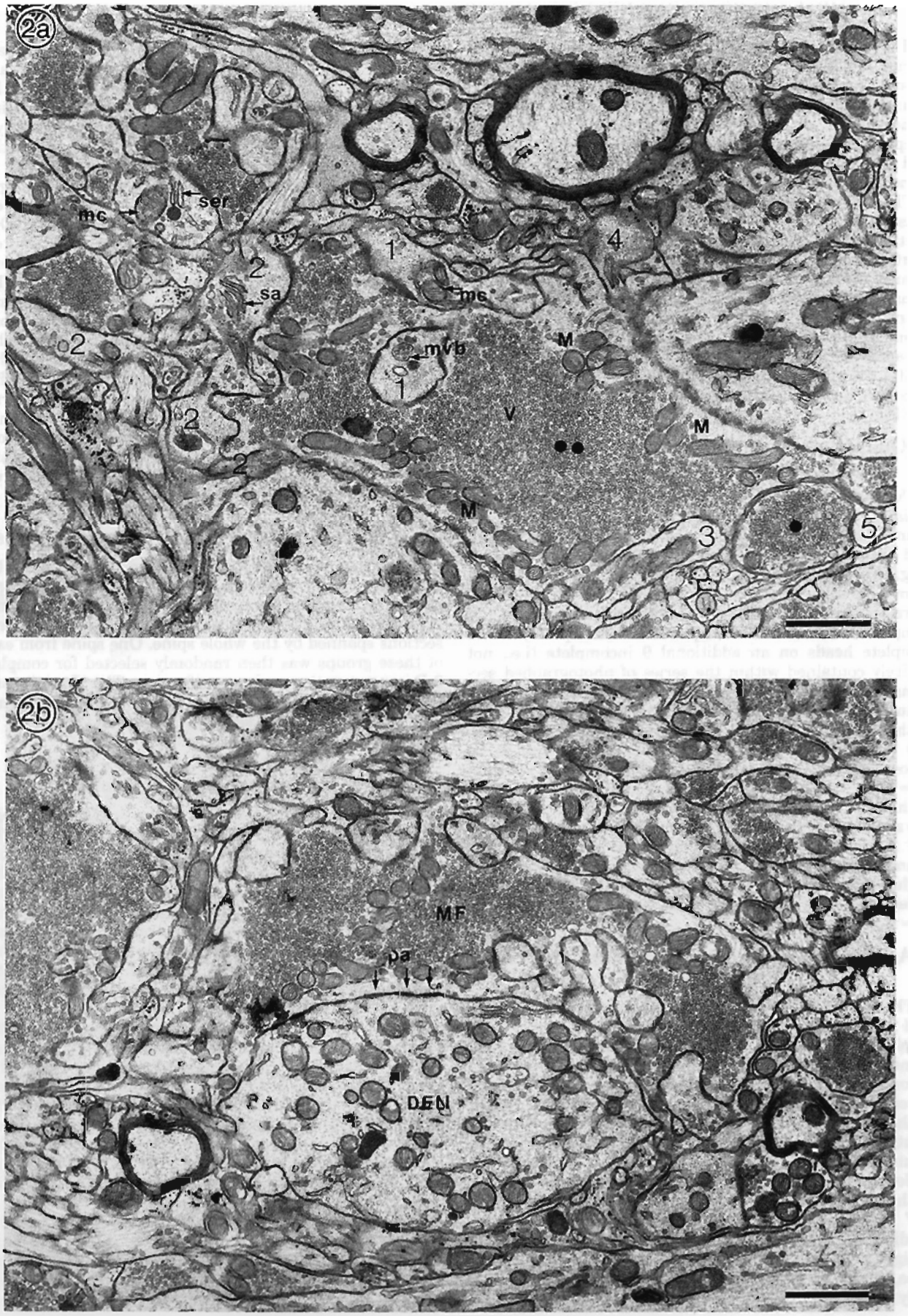

Figure 2

DISCUSSION

The complete reconstructions obtained here provide the first quantitative analysis of the CA3 branched spines and extend previous observations of their subcellular complexity (Blackstad and Kjaerheim, '61; Amaral and Dent, '81). These branched spines from rat hippocampal area CA3 are similar to those from rabbit, cat, and guinea pig in the complexity of their geometry and subcellular composition, and in the location of the MF synapses predominantly on the apical dendrites (Blackstad and Kjaerheim, '61; Hamlyn, '61, '62; Tombol et al., '78; Frotscher, '85). In contrast, primate MF boutons make extensive contacts with branched spines on both the apical and basilar dendrites with CA3 branched spines that appear in single sections to have an even more complex geometry (Frotscher et al., '88). Similar branched spines are found on the proximal dendrites of rat and primate mossy cells in the fascia dentata which are also contacted by the MF boutons (Frotscher et al., '91). The data presented here were obtained from a single rat, though the spines were similar in shape and subcellular constituents as compared with those described in earlier studies (Blackstad and Kjaerheim, '61; Amaral and Dent, '81); thus, the complete 3-D analyses are also likely to be representative of a wide range of branched CA3 spines.

CA3 branched spines are characterized by a unique geometry and ultrastructural composition

Both the geometry and the ultrastructural composition of the CA3 branched spines are markedly different from those of other spine types. Several constituents which are either rare or absent in most spine types are found in relative abundance in the CA3 branched spines. The distance from the spine origin at the dendrite to the PSDs of the MF synapses on the CA3 branched spines averages 2.94 μm and ranges up to 6.52 μm. In contrast, the average distance from the spine origin to the PSD on hippocampal CA1 spines is 0.83 μm (Harris and Stevens, '89), for cerebellar spines it is 1.19 μm (Harris and Stevens, '88), and for visual cortical spines it is 1.46 μm (Spacek and Hartmann, '83). Thus, the relatively greater distances from dendritic sources of metabolic energy and protein synthesis might explain why mitochondria and ribosomes are found more frequently within the individual heads of the CA3 branched spines than in spines of other brain regions.

The abundance of free ribosomes in the branched spines suggests an important role for local protein synthesis that does not require rough endoplasmic reticulum (RER). Although polyribosomes are observed in other types of spines (in 13% of cerebellar spines [Spacek, '85]; in 20% of dentate gyrus spines [Steward, '83]; and in 82% of visual cortical spines [Spacek, '85]), in the CA3 branched spines they are particularly abundant (95%). Earlier studies have shown an increase in the frequency of polyribosomes associated with the bases of dendritic spines in hippocampal granule cells during reinnervation after entorhinal lesions, suggesting a functional correlation between polyribosomes and synaptogenesis (Steward and Levy, '82; Steward, '83). In addition, Desmond and Levy ('90) have reported a decrease in the frequency of polyribosomes at spine bases following LTP, suggesting a modification of translational processes at synapses after LTP.

Very little is known, however, about the mRNA population associated with these polyribosomes. Polyribosomes are rarely associated with membranous cisterns in the branched spines, suggesting a paucity of mRNAs requiring RER for their translation in the spine. Since each MF bouton closely surrounds all the heads of the branched spines, it has been possible to physically separate branched spines from the parent dendrites (Terrian et al., '88). This enriched preparation of CA3 branched spines has been recently found to have a restricted population of mRNA species that code for dendritic soluble proteins such as Ca^{2+}-calmodulin-dependent protein kinase II and MAP-2 (Chicurel et al., '92). In addition, there was an absence of mRNAs that require RER for their translation (for example, synaptophysin and glutamate receptor mRNAs). These findings are consistent with the absence of RER in these CA3 branched spines, and in CA1 and dentate gyrus spines (Steward and Reeves, '88). Ribosomes and spinules were found preferentially in the same heads of the CA3 branched spines, possibly indicating growth and/or remodelling that requires new protein synthesis at these sites. Furthermore, this association would support the hypothesis that the spinules serve an intermediate role in the process of branch formation, elimination or reshaping (Tarrant and Routtenberg, '79; Carlin and Siekivitz, '83; Dyson and Jones, '84).

Individual heads of CA3 branched spines also showed a close association between MVBs and SER. The function of MVBs is not entirely clear but studies by Rosenbluth and Wissig ('64) and more recently by Schmied and Holtzman ('87), support their function as part of the endolysosomal system. One might therefore speculate that the association of these vesicular structures with SER is a reflection of membrane lipid and/or protein turnover in the branched spines.

Although absent in most dendritic spines, microtubules were present in some segments of many CA3 branched spines. Microtubules were found only in spines with greater than 4 heads, suggesting that the large size and extensive branching of these CA3 spines might require a more complex cytoskeletal framework to maintain their shape or alter their structure. The microtubules could also be involved in the transport of cellular constituents throughout the branched spines (see Black and Bass, '89 for review).

Association of CA3 dendritic spines with MF boutons

Single MF boutons contact branched spines from only one parent dendrite of a CA3 pyramidal cell. A single bouton can make up to 37 or more synaptic contacts with branched spines from a single CA3 dendrite. This observation provides the first direct evidence that synapses from a single MF-CA3 bouton are limited to a single CA3 dendrite, and is important for understanding that the MF-CA3 projection is both spatially and numerically limited compared with other hippocampal projections (Amaral et al., '90). In addition, we observed that a single branched spine

Fig. 2. CA3 branched spines and their associated MF boutons. Ultrastructural constituents are indicated as in Figure 1. **a:** Branched spines contact MF boutons of different sizes. A large bouton (2 black circles) is shown contacting more branched spines than a small bouton (1 black circle). Numbers refer to the heads of 5 different branched spines. Heads from the same spine have the same number. Vesicular (V) and mitochondrial (M) zones occur within the boutons. mc, mitochondrion; ser, smooth endoplasmic reticulum; sa, spine apparatus; mvb, multivesicular bodies. **2b:** Puncta adherentia (pa) occur between a dendritic shaft (DEN) and a MF bouton (MF). Bars = 1 μm.

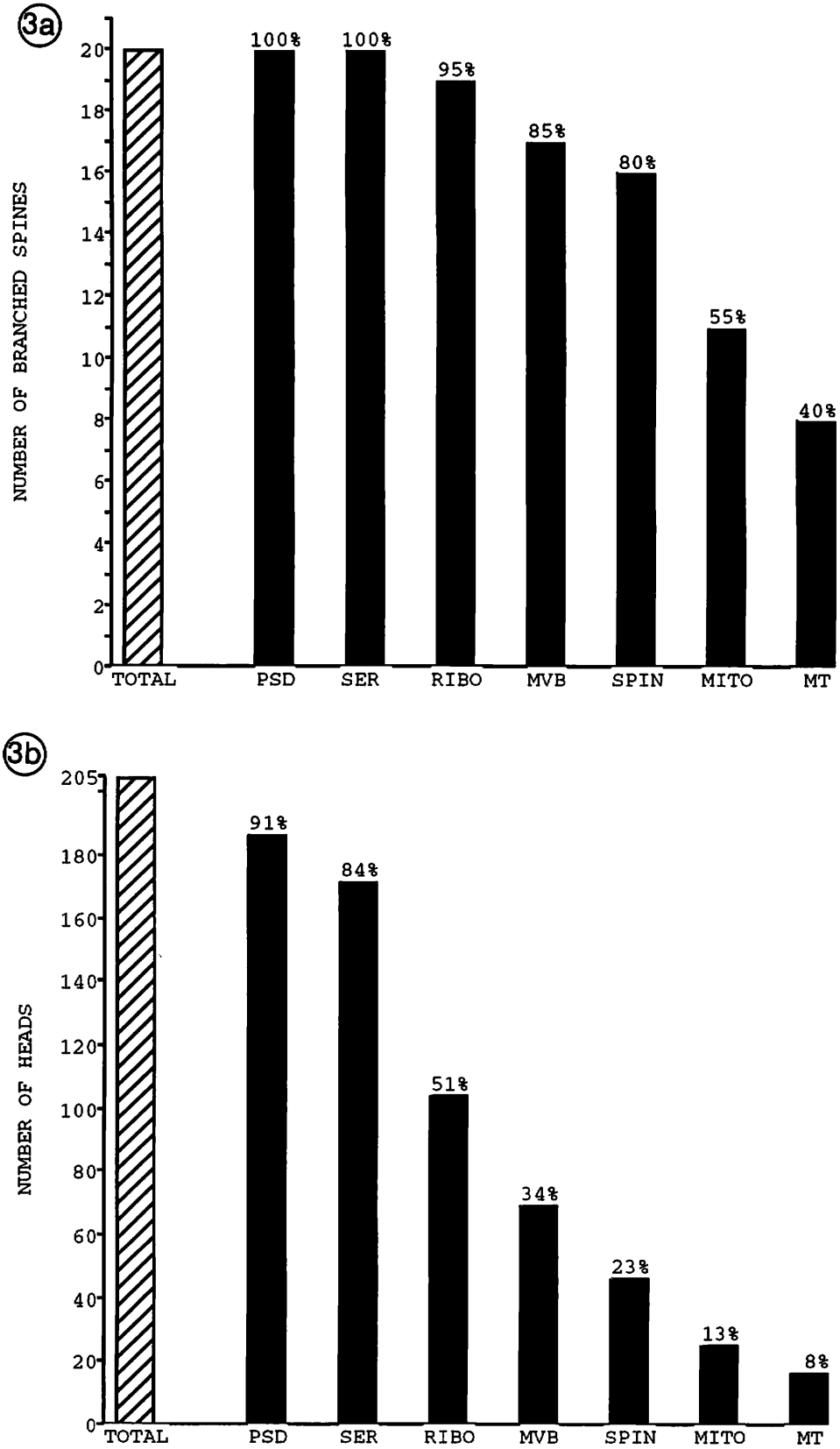

Fig. 3. Quantitative evaluation of the ultrastructural composition of CA3 branched spines. **a:** Presence of ultrastructural components in 20 complete branched spines. **b:** Presence of ultrastructural components within 205 branched spine heads. Heads that were complete within the series from both complete and incomplete spines are included. Abbreviatons: PSD, postsynaptic density; SER, smooth endoplasmic reticulum; RIBO, ribosomes; MVB, multivesicular bodies; SPIN, spinules; MITO, mitochondria; MT, microtubules.

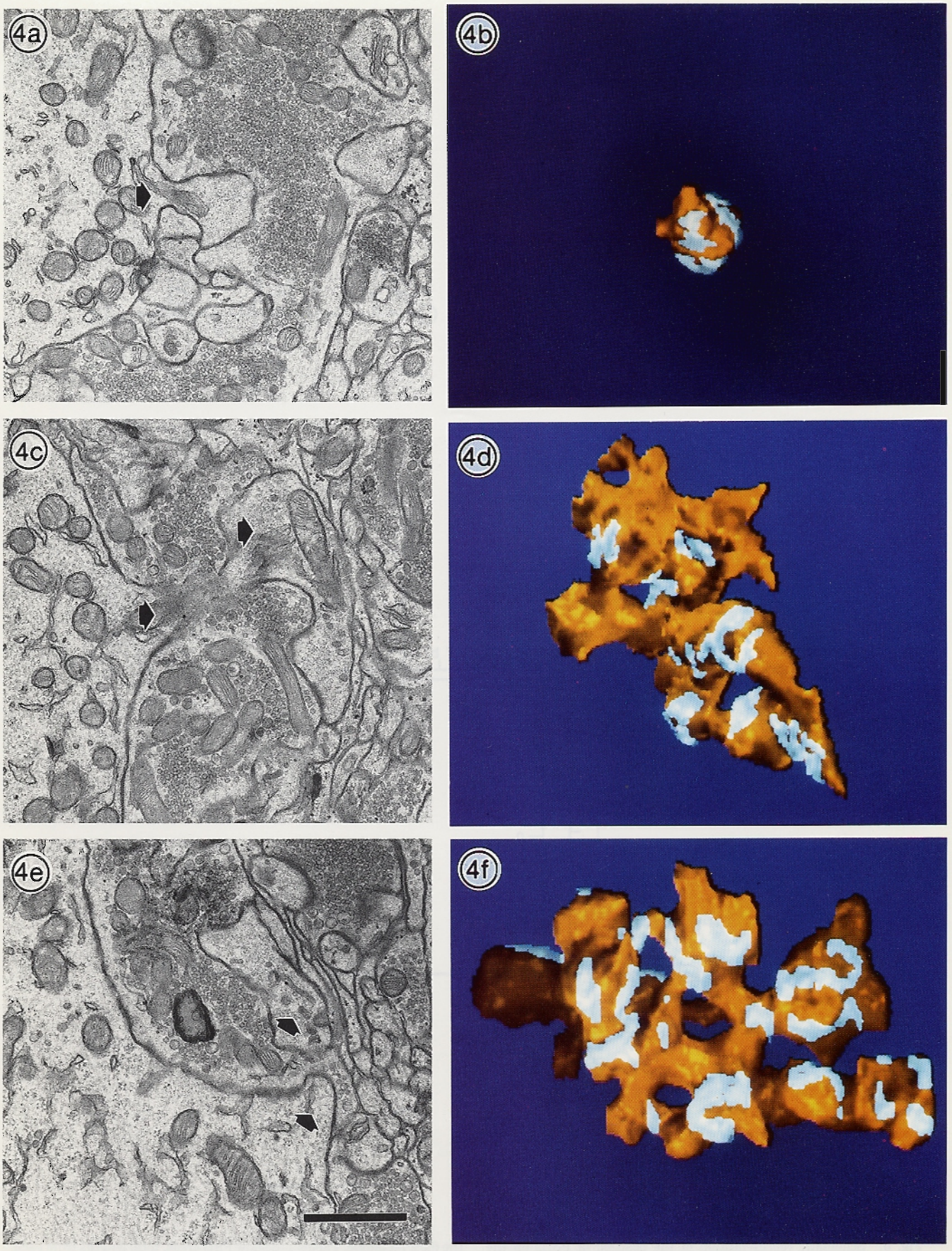

Fig. 4. Complete three-dimensional reconstructions of CA3 branched spines. **a,b:** Micrograph and 3-D reconstruction of a single-headed spine. **c,d:** Micrograph and 3-D reconstruction of an averaged-sized branched spine with 7 heads. **e,f:** Micrograph and 3-D reconstruction of a large branched spine with 12 heads. Spine origins are indicated by arrows in the dendrite, and a portion of the spine heads in c,e is also indicated by an arrow. The origins of the reconstructed spines are at the same relative positions as in the micrographs, on the left side of each image. The reconstructed spines are gold and their PSDs are light blue. Bar in e = 1 μm and applies to a–f.

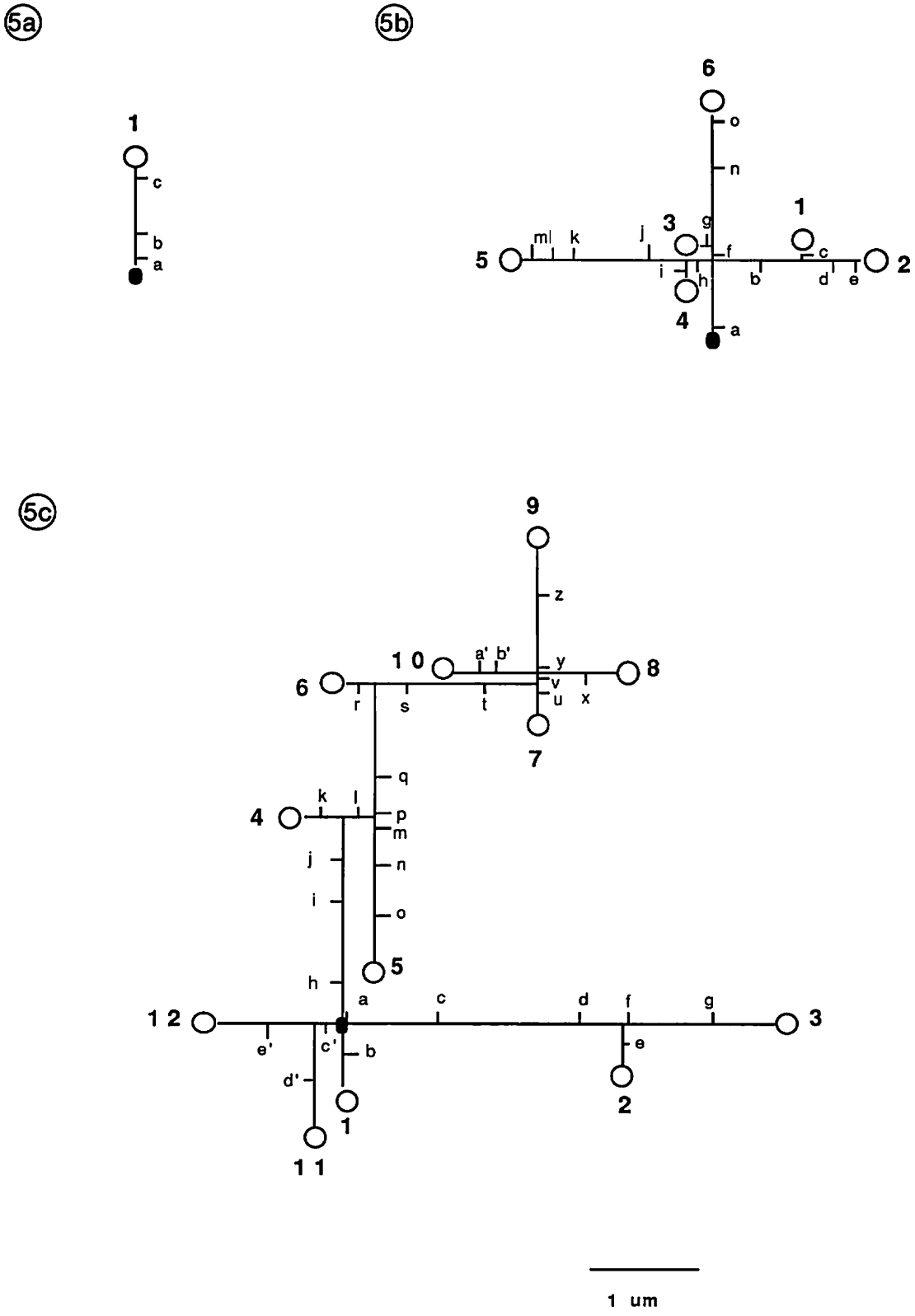

Fig. 5. Schematic representation of the position of PSDs on the reconstructed CA3 spines. Circles represent the PSDs, lines represent the lengths along the spine branches connecting them to the parent dendrite, and the junction with the parent dendrite is represented by the dark rectangle. Tables 1–3 show PSD areas, total lengths from each PSD to the origin of the spine with its parent dendrite, lengths of the branch segments between the letters, and the diameters taken at the positions indicated by the letters.

TABLE 1. Dimensions of Spine in Figure 5A

Head number and position of the diameter	PSD[1] area (μm^2)	Total length[2] (μm)	Segment length[3] (μm)	Diameter[4] (μm)
1c	0.53	0.92	0.15	0.80
1b			0.54	0.72
1a			0.23	0.24

[1]PSD = postsynaptic density.
[2]Total length = total length from the PSD to the origin with the parent dendrite.
[3]Segment length = lengths between positions marked with lower case letters. Of the 2 letters defining a given segment, the letter that is closer to the spine origin is used to identify it in the tables.
[4]The diameter remained essentially uniform along the segment length.

can receive input from more than one MF bouton, but it is not known if these were from the same axon.

The larger the MF boutons are, the more likely they are to synapse with several different branched spines of the same CA3 dendrite, and conversely, the larger the branched CA3 spines are the more likely they are to synapse with multiple MF boutons. At cerebellar and hippocampal area CA1 synapses, the size of the presynaptic axonal bouton is proportional to the number of vesicles it contains, the total area of the PSD, and the volume of the dendritic spine heads for all boutons whether they make 1 or more synapses (Harris and Stevens, '88, '89; Sorra and Harris, '91). Yeow and Peterson ('91) also found that larger boutons make more synapses with motor neurons in the turtle spinal cord. In a variety of systems the number of available postsynaptic sites is important in determining the final number of axonal contacts established in the mature animal (for review see Purves and Lichtman, '85). At the MF-CA3 synapse the size of the presynaptic bouton may *also* regulate the number of synapses that will be associated with it. Frotscher et al. ('77) have observed that the number and size of branched spine profiles decreases when the entorhinal cortex is lesioned during synaptogenesis, suggesting that normal afferent activity to the dentate granule cells may be required for the development of normal CA3 branched spines. Therefore, it is reasonable to extend the

TABLE 2. Dimensions of Reconstructed Spine in Figure 5B.

Head number and position of the diameter	PSD[1] area (μm^2)	Total length[2] (μm)	Segment length[3] (μm)	Diameters[4] T,B,[5]
1c	0.41	1.62	0.04	0.65, 0.85
1b			0.42	0.41
1a			1.16	0.67
2e	0.25	2.06	0.04	0.24, 0.49
2d			0.21	0.51
2b			0.65	0.41
2a			1.16	0.67
3g	0.19	0.69	0.04	0.90
3f			0.06	0.90
3a			0.59	0.67
4i	0.21	1.06	0.11	0.21, 0.68
4h			0.22	0.27
4a			0.73	0.67
5m	0.14	2.47	0.10	0.60
5l			0.25	0.37
5k			0.22	0.43
5j			0.69	0.21, 0.68
5h			0.46	0.27
5a			0.73	0.67
6o	0.08	2.08	0.12	0.99
6n			0.44	0.43
6f			0.93	0.90
6a			0.59	0.67

[1-4]As in Table 1.
[5]T = thin diameter while B = broad diameter where the segment lengths were not cylindrical in shape.

TABLE 3. Dimensions of Reconstructed Spine in Figure 5C

Head No. and Diameter position	PSD[1] area (μm^2)	Total length[2] (μm)	Segment length[3] (μm)	Diameters[4] T,B[5]
1b	0.32	0.57	0.32	0.25
1a			0.25	0.47, 0.83
2e	0.13	3.01	0.20	0.29, 0.51
2d			0.62	0.40, 0.75
2c			1.35	0.29, 0.51
2a			0.84	0.47, 0.83
3g	0.01	4.05	0.60	0.31
3f			0.83	0.17
3d			0.43	0.40, 0.75
3c			1.35	0.29, 0.51
3a			0.84	0.47, 0.83
4k	0.50	2.37	0.15	0.3 7
4j			0.60	0.37
4i			0.38	0.36, 0.89
4h			0.82	0.30
4a			0.42	0.47, 0.83
5o	0.26	3.74	0.47	0.60
5n			0.51	0.29, 0.40
5m			0.35	0.35
5l			0.26	0.44, 0.98
5j			0.53	0.37
5i			0.38	0.36, 0.89
5h			0.82	0.30
5a			0.42	0.47, 0.83
6r	0.19	4.19	0.31	0.60, 1.14
6q			1.06	0.60, 1.14
6p			0.48	0.35
6l			0.19	0.44, 0.98
6j			0.53	0.37
6i			0.38	0.36, 0.89
6h			0.82	0.30
6a			0.42	0.47, 0.83
7u	0.43	5.58	0.22	0.34, 0.57
7t			0.56	0.14
7s			0.78	0.51, 1.11
7q			1.20	0.60, 1.14
7p			0.48	0.35
7l			0.19	0.44, 0.98
7j			0.53	0.37
7i			0.38	0.36, 0.89
7h			0.82	0.30
7a			0.42	0.47, 0.83
8x	0.16	6.24	0.31	0.32
8v			0.52	0.34, 0.57
8t			0.61	0.14
8s			0.78	0.51, 1.11
8q			1.20	0.60, 1.14
8p			0.48	0.35
8l			0.19	0.44, 0.98
8j			0.53	0.37
8i			0.38	0.36, 0.89
8h			0.82	0.30
8a			0.42	0.47, 0.83
9z	0.11	6.53	0.46	0.73
9y			0.69	0.31
9v			0.12	0.34, 0.57
9t			0.46	0.14
9s			0.78	0.51, 1.11
9q			1.20	0.60, 1.14
9p			0.48	0.35
9l			0.19	0.44, 0.98
9j			0.53	0.37
9i			0.38	0.36, 0.89
9h			0.82	0.30
9a			0.42	0.47, 0.83
10a'	0.21	6.24	0.25	0.38, 0.64
10b'			0.16	0.47
10v			0.42	0.34, 0.57
10t			0.61	0.14
10s			0.78	0.51, 1.11
10q			1.20	0.60, 1.14
10p			0.48	0.35
10l			0.19	0.44, 0.98
10j			0.53	0.37
10i			0.38	0.36, 0.89
10h			0.82	0.30
10a			0.42	0.47, 0.83
11d'			0.44	0.35, 1.29
11c'	0.31	1.23	0.64	0.27, 0.47
11a			0.15	0.47, 0.83
12e'			0.44	0.27, 0.47
12c'	0.08	1.19	0.60	0.27, 0.47
12a			0.15	0.47, 0.83

[1-6]See Table 2.

TABLE 4. Comparison of the Dimensions of the Reconstructed CA3 Spines With Spines From Other Brain Regions

Spine type	Volume (μm^3)	Surface area (μm^2)	PSD (μm^2)	PSD:head surface	Head sphericality index[1]
CA3 (1 heads)	0.13	1.70	0.53	—	—
CA3 (6 heads)	1.53	18.90	1.35		
(mean ± S.D. by head)	(0.27 ± 0.12)	(2.36 ± 0.84)	(0.21 ± 0.11)	0.09 ± 0.04	0.67 ± 0.18
CA3 (12 heads)	1.83	22.65	2.72	—	—
Cerebellum[2]	0.12	1.17	0.12	0.13	1.00
Visual cortex[3]	0.21	2.08	0.21	—	—
CA1[4]	0.03	0.63	0.05	0.11	0.85
Neostriatum[5]	0.12	1.46	—	0.13	—

[1]In determining the surface areas, there is a slight experimental measurement error that can be attributed to the difficulty in recognizing boundary surface areas in electron micrographs (Harris and Stevens, '88). Therefore, the sphericality values have been normalized to the cerebellar spine heads because it was shown in an earlier study that these can be considered nearly spherical. By normalizing to a spine head that is known to be very close to spherical, the experimental measurement error is minimized across spines.
[2]From Harris and Stevens ('88).
[3]From Spacek and Hartmann ('83).
[4]From Harris and Stevens ('89) (tissue from the same animal was included in this study).
[5]From Wilson et al. ('83).
— = not determined.

developmental hypothesis of competitive interactions in the formation of neural connections to include the effective size of the presynaptic bouton as a factor contributing to the number of synapses formed with an individual cell.

In all brain regions studied to date, the PSD area has been found to occupy on average 10–15% of the head membrane. The conservation of this ratio both within a single population of spines, across spines from different brain regions, and during development (Harris et al., '92), strongly suggests the existence of either a structural constraint or an optimization in synaptic function. Perhaps there exists a restricted range in the proportion of proteins found at the spine PSD (transmitter receptor molecules, kinase proteins, etc.) to those found at nonsynaptic membrane (voltage-gated ion channels, pumps, structural proteins, etc.) that is optimal for synaptic function, and therefore this ratio must be conserved (see also Hillman et al., '91; Mihaly et al., '91).

Importance of CA3 dendritic spine dimensions to biophysical modelling of postsynaptic physiology

Several biophysical models have addressed the possible ways that dendritic spine dimensions could modulate charge transfer from the synapse to the parent dendrite (Chang, '52; Diamond et al., '70; Rall, '70, '74, '78; Perkel, '82–83; Koch and Poggio, '83; Kawato et al., '84; Turner, '84; Wilson, '84; Perkel and Perkel, '85). However, these models have dealt exclusively with nonbranched spines and have assumed the spine heads to be spherical. Although these assumptions are generally valid for cerebellar, CA1, and neostriatal spines (Wilson, '84; Harris and Stevens, '88, '89), the present study shows this not to be the case for the CA3 branched spines. It is of interest to note, however, that the diameters along the branched spines are greater than the average diameters of unbranched spines in other brain regions. These wide diameters would be less likely to reduce charge transfer from the MF-CA3 synapses, where the peak synaptic conductances are also thought to be greater than at other unbranched spines (Johnston and Brown, '83; Barrioneuvo et al., '86; Bekkers et al., '90). Based on earlier theoretical models, no individual segment of any reconstructed spine was long or constricted enough to reduce charge transfer (Wilson, '84; Harris and Stevens, '88, '89). How the unusual geometry of these branched spines and their association with more than one bouton influence their properties of synaptic transmission and plasticity can now be evaluated in models that utilize the anatomical constraints provided here.

ACKNOWLEDGMENTS

Dr. John Stevens and Dr. Michael Greenberg and ISG Technologies of Canada are thanked for the use of an early, prerelease version of ICAR 80.8 to prepare and display the reconstructions of the dendritic spines. Dr. Huntington Potter is thanked for his helpful comments on an earlier version of the manuscript. Dr. David Jaffe is thanked for reading this paper to establish that sufficient anatomical parameters are presented to create a biophysical model of these spines. This work is supported by NIH-NINCDS-NS21184 (K.M. Harris), The Alfred P. Sloan Foundation (K.M. Harris), a Howard Hughes Medical Institute Predoctoral Fellowship (M.E. Chicurel), NIH-AG09665 (Dr. Huntington Potter, P.I.), and by the MR Center grant P30-HD18655 from NICHD. Portions of this research have been presented in abstract form (Chicurel and Harris, '89).

LITERATURE CITED

Amaral, D.G. (1979) Synaptic extensions from the mossy fibers of the fascia dentata. Anat. Embryol. *155*:241–251.

Amaral, D.G., and J.A. Dent (1981) Development of the mossy fibers of the dentate gyrus: I. A light and electron microscopic study of the mossy fibers and their expansions. J. Comp. Neurol. *195*:51–86.

Amaral, D.G., N. Ishizuka, and B. Claiborne (1990) Neurons, numbers and the hippocampal network. Prog. Brain Res. *83*:1–11.

Barrionuevo, G., S.R. Kelso, D. Johnston, and T.H. Brown (1986) Conductance mechanism responsible for long-term potentiation in monosynaptic and isolated excitatory synaptic inputs to hippocampus. J. Neurophysiol. *55*:540–550.

Bekkers, J.M., G.B. Richerson, and C.F. Stevens (1990) Origin of variability in quantal size in cultured hippocampal neurons and hippocampal slices. Proc. Natl. Acad. Sci. U.S.A. *87*:5359–5362.

Ben-Ari, Y., and A. Represa (1990) Brief seizure episodes induce long-term potentiation and mossy fibre sprouting in the hippocampus. Trends Neurosci. *13*:312–318.

Black, M.M., and P.W. Bass (1989) The basis of polarity in neurons. Trends Neurosci. *12*:211–214.

Blackstad, T.W., and A. Kjaerheim (1961) Special axo-dendritic synapses in the hippocampal cortex: Electron and light microscopic studies on the layer of mossy fibers. J. Comp. Neurol. *117*:133–159.

Bliss, T.V.P., S.H. Chung, and R.V. Stirling (1974) Structural and functional development of the mossy fibre system in the hippocampus of the post-natal rat. J. Physiol. (Lond) *239*:92P–93P.

Bradler, J.E., and G. Barrionuevo (1989) Long-term potentiation in hippocampal CA3 neurons: Tetanized input regulates heterosynaptic efficacy. Synapse *4*:132–142.

Bradler, J.E., and G. Barrionuevo (1990) Heterosynaptic correlates of long-term potentiation induction in hippocampal CA3 neurons. Neuroscience *35*:265–271.

Brown, T.H., V.C. Chang, A.H. Ganong, C.L. Keenan, and S.R. Kelso (1988) Biophysical properties of dendrites and spines that may control the induction and expression of long-term synaptic potentiation. In P.W. Landfield and S.A. Deadwyler (eds): Long-term Potentiation: From Biophysics to Behavior. Neurology and Neurobiology Volume 35. New York: Alan R. Liss, pp. 201–264.

Carlin, R.K., and P. Siekevitz (1983) Plasticity in the central nervous system: Do synapses divide? Proc. Natl. Acad. Sci. U.S.A. *80*:3517–3521.

Chang, H.T. (1952) Cortical neurons with particular reference to the apical dendrites. Cold Spring Harbor Symposium Quant. Biol. *17*:189–202.

Chicurel, M.E., and K.M. Harris (1989) Serial electron microscopy of CA3 dendritic spines synapsing with mossy fibers of rat hippocampus. Soc. Neurosci. Abs. *15*:256.

Chicurel, M.E., D.M. Terrian, and H. Potter (1992) mRNA at the synapse: Analysis of a synaptosomal preparation enriched in hippocampal dendritic spines. (submitted).

Claiborne, B.J., D.G. Amaral, and W.M. Cowan (1986) A light and electron microscopic analysis of the mossy fibers of the rat dentate gyrus. J. Comp. Neurol. *246*:435–458.

Coss, R.G., and D.H. Perkel (1985) The function of dendritic spines: A review of theoretical issues. Behav. Neural Biol. *44*:151–185.

Desmond, N.L., and W.B. Levy (1990) Morphological correlates of long-term potentiation imply the modification of existing synapses, not synaptogenesis, in the hippocampal dentate gyrus. Synapse *5*:139–143.

Diamond, J., E.G. Gray, and G.M. Yasargil (1970) The function of the dendritic spine: An hypothesis. In P. Andersen and J.K.S. Jensen (eds): Excitatory Synaptic Mechanisms. Oslo, Norway: Universitets Forlaget, pp. 213–222.

Dyson, S.E., and D.G. Jones (1984) Synaptic remodelling during development and maturation: Junction differentiation and splitting as a mechanism for modifying connectivity. Dev. Brain Res. *13*:125–137.

Freeman, E.J., D.M. Terrian, and R.V. Dorman (1990) Presynaptic facilitation of glutamate release from isolated hippocampal mossy fiber nerve endings by arachidonic acid. Neurochem. Res. *15*:743–750.

Frotscher, M. (1985) Mossy fibres form synapses with identified pyramidal basket cells in the CA3 region of the guinea-pig hippocampus: A combined Golgi-electron microscope study. J. Neurocytol. *14*:245–259.

Frotscher, M., J. Hamori, and J. Wenzel (1977) Transneuronal effects of entorhinal lesions in the early postnatal period on synaptogenesis in the hippocampus of the rat. Exp. Brain. Res. *30*:549–560.

Frotscher, M., J. Kraft, and U. Zorn (1988) Fine structure of identified neurons in the primate hippocampus: A combined Golgi/EM study in the baboon. J. Comp. Neurol. *275*:254–270.

Frotscher, M., L. Seress, W.K. Schwerdtfeger, and E. Buhl (1991) The mossy cells of the fascia dentata: A comparative study of their fine structure and synaptic connections in rodents and primates. J. Comp. Neurol. *312*:145–163.

Gaarskjaer, F.B. (1986) The organization and development of the hippocampal mossy fiber system. Brain Res. Rev. *11*:335–357.

Gall, C. (1988) Seizures induce dramatic and distinctly different changes in enkephalin, dynorphin, and CCK immunoreactives in mouse hippocampal mossy fibers. J. Neurosci. *8*:1852–1862.

Gamble, E., and C. Koch (1987) The dynamics of free calcium in dendritic spines in response to repetitive synaptic input. Science *236*:1311–1315.

Hamlyn, L.H. (1961) Electron microscopy of mossy fibre endings in Ammon's horn. Nature *190*:645–646.

Hamlyn, L.H. (1962) The fine structure of the mossy fibre endings in the hippocampus of the rabbit. J. Anat. *96*:112–120.

Harris, E.W., and C.W. Cotman (1986) Long-term potentiation of guinea pig mossy fiber responses in not blocked by N-methyl-D-aspartate antagonists. Neurosci. Lett. *70*:132–137.

Harris, K.M., and J.K. Stevens (1988) Dendritic spines of rat cerebellar Purkinje cells: Serial electron microscopy with reference to their biophysical characteristics. J. Neurosci. *8*:4455–4469.

Harris, K.M., and J.K. Stevens (1989) Dendritic spines of CA1 pyramidal cells in the rat hippocampus: Serial electron microscopy with reference to their biophysical characteristics. J. Neurosci. *9*:2982–2997.

Harris, K.M., F.E. Jensen, and B. Tsao (1992) Three-dimensional structure of dendritic spines and synapses in rat hippocampus (CA1) at postnatal day 15 and adult ages: Implications for the maturation of synaptic physiology and long-term potentiation. J. Neurosci. *12*:2685–2705

Hillman, D., S. Chen, T.T. Aung, B. Cherksey, M. Sugimori, and R.R. Llinas (1991) Localization of P-type calcium channels in the central nervous system. Proc. Natl. Acad. Sci. U.S.A. *88*:7076–7080.

Hoffman, D.W., and N. Zamir (1984) Localization and quantitation of dynorphin B in the rat hippocampus. Brain Res. *324*:354–357.

Hopkins, W.F., and D. Johnston (1988) Noradrenergic enhancement of long-term potentiation at mossy fiber synapses in the hippocampus. J. Neurophysiol. *59*:667–687.

Ibata, Y., and N. Otsuka (1969) Electron microscopic demonstration of zinc in the hippocampal formation using Timm's sulfide-silver technique. J. Histochem. Cytochem. *17*:171–175.

Ito, I., D. Okada, and H. Sugiyama (1988) Pertussis toxin suppresses long-term potentiation of hippocampal mossy fiber synapses. Neurosci. Lett. *90*:181–185.

Jaffe, D., and D. Johnston (1990) Induction of long-term potentiation at hippocampal mossy-fiber synapses follows a Hebbian rule. J. Neurophysiol. *64*:948–960.

Johnston, D., and T.H. Brown (1983) Interpretation of voltage-clamp measurements in hippocampal neurons. J. Neurophysiol. *50*:464–486.

Kamiya, H., S. Sawada, and C. Yamamoto (1988) Additive feature of long-term potentiation and phorbol ester-induced synaptic enhancement in the mossy fiber-CA3 synapse. Exp. Neurol. *102*:314–317.

Kawato, M., T. Hamaguchi, F. Murakami, and N. Tsukahara (1984) Quantitative analysis of electrical properties of dendritic spines. Biol. Cybern. *50*:447–454.

Koch, C., and T. Poggio (1983) A theoretical analysis of electrical properties of spines. Proc. R. Soc. (Lond.) *218*:455–477.

McGinty, J.F., S.J. Henriksen, A. Goldstein, L. Terenius, and F.E. Bloom (1983) Dynorphin is contained within hippocampal mossy fibers: Immunocytochemical alterations after kainic acid administration and colchicine-induced neurotoxicity. Proc. Natl. Acad. Sci. U.S.A. *80*:589–593.

Mihaly, A., T. Oravecz, Z. Olah, and U.R. Rapp (1991) Immunohistochemical localization of raf protein kinase in dendritic spines and spine apparatuses of the rat cerebral cortex. Brain Res. *547*:309–314.

Morris, B.J., K.J. Feasey, G.T. Bruggencate, A. Herz, and V. Hollt (1988) Electrical stimulation *in vivo* increases the expression of proenkephalin mRNA and decreases the expression of prodynorphin mRNA in rat hippocampal granule cells. Proc. Natl. Acad. Sci. U.S.A. *85*:3226–3230.

Moshkov, D.A., L.L. Petrovskaya, and A.G. Bragin (1977) Posttetanic changes in the ultrastructure of the giant spinous synapses in area CA3 of the hippocampus. Doklady Akademii Nauk SSSR *237*:1525–1528.

Okada, D., S. Yamagishi, and H. Sugiyama (1989) Differential effects of phospholipase inhibitors in long-term potentiation in the rat hippocampal mossy fiber synapses and Schaffer/commissural synapses. Neurosci. Lett. *100*:141–146.

Pearlstein, R.A., L. Kirschner, J. Simons, S. Machell, W.F. White, and R.L. Sidman (1986) A multimodal system for reconstruction and quantification of neurologic structures. Anal. Quant. Cytol. Histol. *8*:108–115.

Perkel, D.H. (1982–1983) Functional role of dendritic spines. Physiologie (Paris) *78*:695–699.

Perkel, D.H., and D.J. Perkel (1985) Dendritic spines: Role of active membrane in modulating synaptic efficacy. Brain Res. *325*:331–335.

Petukhov, D.H., and V.I. Popov (1986) Quantitative analysis of ultrastructural changes in synapses of the rat hippocampal field CA3 *in vitro* in different functional states. Neuroscience *18*:823–835.

Purves, D., and J.W. Lichtman (1985) Principles of Neural Development. Sunderland, MA: Sinauer Assoc. Inc., pp. 271–300.

Rall, W. (1970) Cable properties of dendrites and effects of synaptic location. In P. Andersen and J.K.S. Jensen (eds): Excitatory Synaptic Mechanisms. Oslo: Universitets Forlaget, pp. 175–187.

Rall, W. (1974) Dendritic spines, synaptic potency, and neuronal plasticity. In C. Woody, K. Brown, T. Crow, and J. Knispel (eds): Cellular Mechanisms Subserving Changes in Neuronal Activity. Los Angeles: Brain Information Service, pp. 13–21.

Rall, W. (1978) Dendritic spines and synaptic potency. In A.K. McIntyre and K. Porter (eds): Studies in Neurophysiology. Cambridge, England: Cambridge Univ. Press, pp. 203–209.

Rall, W., and I. Segev (1988) Synaptic integration and excitable dendritic spine clusters: Structure/function. Neurol. and Neurobiol. *37*:263–282.

Ramon y Cajal, S. (1911) Histologie du System Nerveux de l'Homme et des Vertebres. Vol. II, Paris: Maloine.

Regehr, W.G., and D.W. Tank (1991) The maintenance of LTP at hippocampal mossy fiber synapses is independent of sustained presynaptic calcium. Neuron *7*:451–459.

Rosenbluth, J., and S.L. Wissig (1964) The distribution of exogenous ferritin in toad spinal ganglia and the mechanism of its uptake by neurons. J. Cell Biol. *23:*307–325.

Sandler, R., and D. Smith (1991) Coexistence of GABA and glutamate in mossy fiber terminals of the primate hippocampus: An ultrastructural study. J. Comp. Neurol. *303:*177–192.

Schmied, R., and E. Holtzman (1987) A phosphatase activity and synaptic vesicle antigen in multivesicular bodies of frog retinal photoreceptor terminals. J. Neurocytol. *16:*627–637.

Sokal, R.R., and J.F. Rohlf (1981) Biometry. New York: W.H. Freeman and Co.

Sorra, K.E., and K.M. Harris (1991) Multiple contacts between hippocampal CA3 axons and apical dendrites of CA1 pyramidal cells. Soc. Neurosci. Abstr. *459:*8.

Spacek, J. (1985) Three-dimensional analysis of dendritic spines. II. Spine apparatus and other cytoplasmic components. Anat. Embryol. *171:*235–243.

Spacek, J., and M. Hartmann (1983) Three-dimensional analysis of dendritic spines: I. Quantitative observations related to dendritic spine and synaptic morphology in cerebral and cerebellar cortices. Anat. Embryol. *167:*289–310.

Staubli, U., J. Larson, and G. Lynch (1990) Mossy fiber potentiation and long-term potentiation involve different expression mechanisms. Synapse *5:*333–335.

Stevens, J.K., and J. Trogadis (1984) Computer assisted reconstruction from serial electron micrographs. Ann. Rev. Neurobiol. *5:*341–369.

Steward, O. (1983) Alterations in polyribosomes associated with dendritic spines during the reinnervation of the dentate gyrus of the adult rat. J. Neurosci. *3:*177–188.

Steward, O., and W.B. Levy (1982) Preferential localization of polyribosomes under the base of dendritic spines in granule cells of the dentate gyrus. J. Neurosci. *2:*284–291.

Steward, O., and T.M. Reeves (1988) Protein-synthetic machinery beneath postsynaptic sites on CNS neurons: Association between polyribosomes and other organelles at the synaptic site. J. Neurosci. *8:*176–184.

Storm-Mathisen, J., A.K. Leknes, A.T. Bore, J.L. Vaaland, P. Edminson, F.S. Haug, and O.P. Ottersen (1983) First visualization of gluatamate and GABA in neurones by immunocytochemistry. Nature *301:*517–520.

Tarrant, S.B., and A. Routtenberg (1979) Postsynaptic membrane and spine apparatus: Proximity in dendritic spines. Neurosci. Lett. *11:*289–294.

Terrian, D., R.L. Gannon, and M.A. Rea (1990) Glutamate is the endogenous amino acid selectively released by rat hippocampal mossy fiber synaptosomes concomitantly with prodynorphin-derived peptides. Neurochem. Res. *15:*1–5.

Terrian, D.M., P.G. Hernandez, M.A. Rea, and R.I. Peters (1989) ATP release, adenosine formation and modulation of dynorphin and glutamic acid release by adenosine analogues in rat hippocampal mossy fiber synaptosomes. J. Neurochem. *53:*1390–1399.

Terrian, D.M., D. Johnston, B.J. Claiborne, R. Ansah-Yiadom, W.J. Strittmatter, and M.A. Rea (1988) Glutamate and dynorphin release from a subcellular fraction enriched in hippocampal mossy fiber synaptosomes. Brain Res. Bull. *21:*343–351.

Tombol, T., G. Somogyi, and M. Madarasz (1978) Granule cells, mossy fibres and pyramidal neurons: An electron microscopic study of the cat's hippocampal formation, I. Acta Morphologica Acad. Sci. Hung *26:*291–310.

Turner, D.A. (1984) Conductance transients onto dendritic spines in a segmental cable model of hippocampal neurons. Biophys. J. *46:*85–96.

Wickens, J. (1988) Electrically coupled but chemically isolated synapses: Dendritic spines and calcium in a rule for synaptic modification. Prog. Neurobiol. *31:*507–528.

William, S., and D. Johnston (1988) Muscarinic depression of long-term potentiation in CA3 hippocampal neurons. Science *242:*84–87.

Williams, S., and D. Johnston (1989) Long-term potentiation of hippocampal mossy fiber synapses is blocked by postsynaptic injection of calcium chelators. Neuron *3:*583–588.

Wilson, C.J. (1984) Passive cable properties of dendritic spines and spiny neurons. J. Neurosci. *4:*281–297.

Wilson, C.J., P.M. Groves, S.T. Kitai, and J.C. Linder (1983) Three dimensional structure of dendritic spines in the rat neostriatum. J. Neurosci. *3:*383–398.

Xiang, Z., E.W. Kairiss, C.L. Keenan, E.M. Landaw, and T.H. Brown (1990) Quantal model of synaptic current fluctuations in hippocampal neurons. Soc. Neurosci. Abs. *212.11:*492.

Yeow, M.G.L., and E.H. Peterson (1991) Active zone organization and vesicle content scale with bouton size at a vertebrate central synapse. J. Comp. Neurol. *307:*475–486.

Zalutsky, R.A., and R.A. Nicoll (1990) Comparison of two forms of long-term potentiation in single hippocampal neurons. Science *248:*1619–1624.